

See discussions, stats, and author profiles for this publication at: <https://www.researchgate.net/publication/274643280>

# High-Throughput, Quantitative Enzyme Kinetic Analysis in Microdroplets Using Stroboscopic Epifluorescence Imaging

ARTICLE *in* ANALYTICAL CHEMISTRY · APRIL 2015

Impact Factor: 5.64 · DOI: 10.1021/acs.analchem.5b00766 · Source: PubMed

---

READS

4

## 4 AUTHORS, INCLUDING:



Stavros Stavrakis

ETH Zurich

16 PUBLICATIONS 272 CITATIONS

[SEE PROFILE](#)

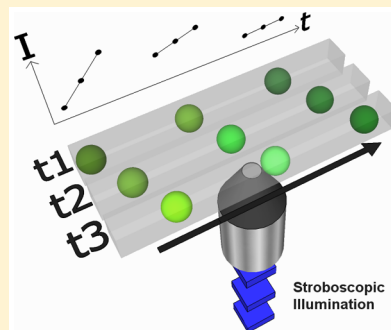
# High-Throughput, Quantitative Enzyme Kinetic Analysis in Microdroplets Using Stroboscopic Epifluorescence Imaging

David Hess, Anandkumar Rane, Andrew J. deMello,\* and Stavros Stavrakis

Institute for Chemical and Bioengineering, Department of Chemistry and Applied Biosciences, ETH Zürich, Vladimir Prelog Weg 1, 8093 Zürich, Switzerland

 Supporting Information

**ABSTRACT:** Droplet-based microfluidic systems offer a range of advantageous features for the investigation of enzyme kinetics, including high time resolution and the ability to probe extremely large numbers of discrete reactions while consuming low sample volumes. Kinetic measurements within droplet-based microfluidic systems are conventionally performed using single point detection schemes. Unfortunately, such an approach prohibits the measurement of an individual droplet over an extended period of time. Accordingly, we present a novel approach for the extensive characterization of enzyme–inhibitor reaction kinetics within a single experiment by tracking individual and rapidly moving droplets as they pass through an extended microfluidic channel. A series of heterogeneous and pL-volume droplets, containing varying concentrations of the fluorogenic substrate resorufin  $\beta$ -D-galactopyranoside and a constant amount of the enzyme  $\beta$ -galactosidase, is produced at frequencies in excess of 150 Hz. By stroboscopic manipulation of the excitation laser light and adoption of a dual view detection system, “blur-free” images containing up to 150 clearly distinguishable droplets per frame are extracted, which allow extraction of kinetic data from all formed droplets. The efficiency of this approach is demonstrated via a Michaelis–Menten analysis which yields a Michaelis constant,  $K_m$ , of 353  $\mu\text{M}$ . Additionally, the dissociation constant for the competitive inhibitor isopropyl  $\beta$ -D-1-thiogalactopyranoside is extracted using the same method.



Droplet-based microfluidic systems have attracted much attention in recent years as core platforms for biological experimentation due to the distinctive features of small volume compartmentalization, high analytical throughput, and the ability to precisely control the droplet payload.<sup>1</sup> Indeed, a diversity of studies have elegantly demonstrated the potential of such technology in a range of applications including enzymatic assays,<sup>2–5</sup> single cell screens,<sup>6–9</sup> digital PCR,<sup>10</sup> and the bespoke synthesis of monodisperse nanomaterials.<sup>11–13</sup>

When coupled with fluorescence microscopy, droplet-based microfluidic systems provide a powerful platform for enzyme kinetics studies.<sup>2,4</sup> For example, by leveraging rapid and chaotic mixing of reagents within pL-volume droplets, Song and Ismagilov demonstrated enzyme kinetic measurements with millisecond time resolution.<sup>2</sup> At a basic level, the study of enzyme kinetics enables the elucidation of the mechanism of enzymatic action with the continuous addition of an inhibitor controlling the rate of the specific enzyme-catalyzed process.<sup>14</sup> Conventional methods for determining kinetic parameters such as  $K_m$  (the Michaelis constant),  $V_{\max}$  (the maximum rate), and  $k_{\text{cat}}$  (the turnover number) typically involve observation of multiple and independent reactions in well-based formats where the concentrations of enzyme and substrate are varied in a systematic manner.<sup>15</sup> The requisite operations are time-consuming and labor intensive and expend excessive sample and reagent volumes. Conversely, the adoption of droplet-based methods affords a dramatic reduction in sample and reagent volumes via compartmentalization within nL to pL

volumes and rapid mixing via chaotic advection.<sup>2</sup> Such features enable the facile creation of concentration gradients and thus a massive expansion in experimental diversity.<sup>4,16</sup> These are significant rewards since enzymes and their associated activators or inhibitors are expensive and normally available in only small amounts. In this respect, a microfluidic gradient generator able to manipulate small volumes of reagents through a network of micrometer-sized channels represents an ideal environment for screening a wide variety of experimental parameters under well-defined mass transport conditions.<sup>3</sup> The realization of microfluidic concentration gradients typically relies on the splitting and recombination of flows,<sup>17</sup> the combination of laminar flows prior to droplet formation,<sup>4</sup> or the exploitation of Taylor-Aris dispersion.<sup>3,16,17</sup> For example, an elegant approach for the production of droplet-based concentration gradients introduced by Ismagilov and co-workers involves the regulation of the flow rate ratio of fluid streams at a microfluidic T junction.<sup>18</sup> Previously, Damean et al. combined droplet microfluidics with wide field fluorescence imaging to simultaneously probe different reactions confined in microdroplets.<sup>17</sup> This approach, although somewhat successful, introduces a range of experimental difficulties. These include complex fluidic channel networks and limited multiplexing capabilities (since screening

Received: February 26, 2015

Accepted: April 7, 2015

Published: April 7, 2015

is limited to four different substrate concentrations per experiment). Alternative microfluidic platforms incorporating microvalves and pico-injectors have also been used for the generation of concentration gradients.<sup>19,20</sup> Despite some degree of success, microfluidic valves and injector-based systems are complex to fabricate and are associated with an increased error in injection volumes. In addition, it is important to note that mixing in continuous-flow microfluidic systems is usually dominated by diffusive mass transport, which can be relatively slow. To overcome this problem, a range of passive and active mixing schemes have been developed.<sup>21</sup> Accordingly, mixing within segmented flows is well-defined and can be probed using a variety of mixing assays. This allows for the incorporation of a "mixing function" into the kinetic model.<sup>2</sup> In contrast, conventional stopped-flow approaches fail to take into account the aforementioned phenomenon, resulting in dead times defined by the mixing time.

To date, kinetic analyses using droplet-based microfluidic systems have almost exclusively involved single point detection schemes at defined locations within an extended microfluidic channel,<sup>22–24</sup> or fluorescence-based wide-field imaging of a homogeneous set of (identical) droplets.<sup>2</sup> Unfortunately, the latter approach cannot provide accurate information relating to droplet heterogeneity since only average values are obtained by integrating images over many seconds. Alternatively, tracking individual droplets using wide-field imaging methods can in principle provide information regarding temporal concentration changes but is severely hampered by the fact that the frame rates of high-sensitivity CCD cameras are too low to detect droplets moving at high linear velocities. This makes it difficult to monitor a reaction along an extended microchannel, and unsurprisingly, such an approach has yet to be demonstrated within a droplet-based microfluidic platform.

To address this limitation, we implement herein a combination of droplet-based microfluidics and wide field stroboscopic illumination to probe reaction kinetics in individual droplets along a microfluidic channel. Specifically, we generate a series of droplets, containing different fluorogenic substrate concentrations (barcoded with a fluorescent dye), by varying the flow rate ratio of a stock solution and a diluent prior to droplet formation. As a model system, the Michaelis–Menten kinetics of  $\beta$ -galactosidase are assayed using wide-field fluorescence imaging. Individual droplets are tracked from frame to frame through knowledge of their velocity and the time difference between consecutive images. Such an approach allows for the extraction of kinetic data, by measurement of the signal originating from the product of the enzymatic reaction. As previously noted, high droplet velocities ( $>5$  cm/s) will lead to motion blur when utilizing long detector exposures, which in turn results in a loss of biological information. To overcome this problem, a sensitive CMOS camera in combination with stroboscopic excitation is used to introduce microsecond excitation pulses, thus reducing associated motion blur. By synchronizing light modulation with the shutter of the camera, effective exposure times can be adequately reduced (down to approximately 20  $\mu$ s), which allows the recording of images that report distinguishable droplets. Moreover, to achieve simultaneous detection of the enzymatic reaction product and the barcoding dye, a dual view optical detection system is implemented. Such a system allows light emitted by two different fluorophores to be projected onto different regions of the detector.

## MATERIALS AND METHODS

**Microfluidic Devices.** Microfluidic channel designs (Figure S1, Supporting Information) were created using AutoCAD (AutoCAD 2014, Autodesk, USA) and printed onto transparent film masks (Micro Lithography Services Ltd., Chelmsford, United Kingdom). SU-8 coated silicon molds of the designs (with feature heights of 50  $\mu$ m) were then fabricated via conventional photolithography. Subsequently, a 10:1 mixture of polydimethylsiloxane (PDMS) and curing agent (Sylgard 184, Dow Corning, Midland MIUSA) was poured onto the mold and cured at 70 °C for 2 h. After curing, the structured PDMS layer was separated from the mold and then diced to yield individual devices with inlet/outlets formed at specific locations using a hole puncher (Technical Innovations, West Palm Beach, FL, USA). Finally, the structured layer was bonded to PDMS covered glass slides (Menzel-Gläser, Braunschweig, Germany) in an oxygen plasma (EMITECH K1000X, Quorum Technologies, East Sussex, United Kingdom). Gastight syringes (1001TLL, Sigma-Aldrich, Buchs, Switzerland) were connected to PTFE tubing (PTFE tube 0.25 mm ID  $\times$  1/16 in. OD, Fisher Scientific, Reinach, Switzerland) via an adapter with the other ends connected to 2 cm long Tygon tubing (TygonS-54-HL ID 250  $\mu$ m, Fisher Scientific, Reinach, Switzerland) directly inserted into the device inlets.

**Enzymatic Assay.** Aqueous solutions were prepared in phosphate buffered saline (pH7, Life Technologies, Zug, Switzerland), to which was added 1 mM MgCl<sub>2</sub> (Sigma-Aldrich, Buchs, Switzerland) and 0.05% v/v Tween 20 (Sigma-Aldrich, Buchs, Switzerland). A custom synthesized biocompatible polyethylene glycol-perfluoropolyether (PEG–PFPE) block copolymer fluorinated surfactant<sup>25</sup> was added to the oil phase (FC-40, ABCR-Chemicals, Karlsruhe, Germany) at 3% w/w. Prior to use, solutions were filtered using a syringe filter (0.2  $\mu$ m PTFE filter, Fisher Scientific, Reinach, Switzerland) and degassed in a desiccator. For kinetic experiments, syringes were filled with solutions of 1 mM resorufin  $\beta$ -D-galactopyranoside (Sigma-Aldrich, Buchs, Switzerland), barcoded with 20  $\mu$ M Atto633 (Sigma-Aldrich, Buchs, Switzerland), 0.2245 mg/mL  $\beta$ -galactosidase from *Escherichia coli* (Grade VIII,  $\geq$ 500 units/mg, Lot SLBF5960 V, Sigma-Aldrich, Buchs, Switzerland), pure buffer, and for the inhibition studies 250  $\mu$ M isopropyl  $\beta$ -D-1-thiogalactopyranoside (Sigma-Aldrich, Buchs, Switzerland). Preliminary experiments investigating the stability of flow profiles were conducted using a 100  $\mu$ M resorufin (Sigma-Aldrich, Buchs, Switzerland) solution and a 15  $\mu$ M CF 647 hydrazide (Sigma-Aldrich, Buchs, Switzerland) solution.

**Device Operation.** Before the operational flow conditions (oil phase: 5  $\mu$ L/min; substrate and dilution buffer: 3  $\mu$ L/min; enzyme: 2  $\mu$ L/min; for inhibition studies, inhibitor and dilution buffer: 2  $\mu$ L/min in total) were applied, devices were initially filled with FC-40 at a flow rate of 2  $\mu$ L/min. Precision syringe pumps (neMESYS Low Pressure Syringe Pump, CETONI GmbH, Korbussen, Germany) were operated using associated software (UserInterface, CETONI GmbH, Korbussen, Germany). To create concentration gradients, complementary periodic flow profiles (keeping a constant total flow rate) were assigned to the two syringes: one containing the substrate and the other pure buffer. The flow profiles consisted of a predefined periodic series of flow rate values used to ramp the syringe pumps in 100 ms steps (Figure 2b). The execution of the two complementary flow profiles was synchronized, and

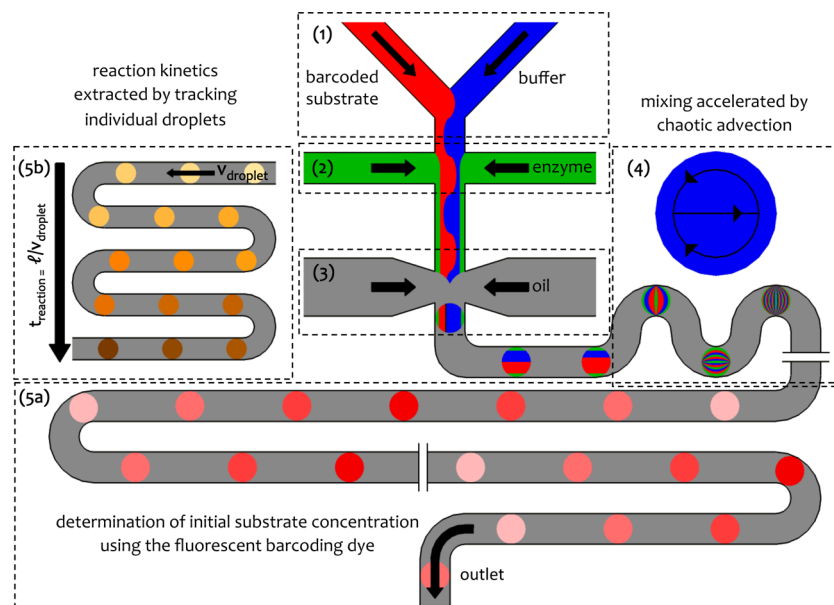


**Figure 1.** A droplet-based enzymatic assay platform. A concentration gradient of barcoded substrate is created by varying the volumetric flow rates of buffer and substrate streams (1). A constant amount of enzyme is then added (2) prior to droplet formation using a flow focusing geometry (3). Rapid mixing inside the droplets is achieved by chaotic advection (4). Droplets containing different substrate concentrations pass through the detection field of view in a serpentine channel, and epifluorescence images are recorded (5a). By tracking individual droplets through each frame, the formation of the fluorescent reaction product can be measured over time (5b).

images were recorded after stable droplet formation was established.

**Fluorescence Detection System.** The optical system consisted of a Nikon Ti-E (Nikon, Zurich, Switzerland) inverted microscope equipped with a motorized stage (Mad City Laboratories, Maddison, USA) and a Dual-View detection system (Cairn Research, Kent, United Kingdom). 640 nm (CUBE 640-100C, Coherent, Ely, United Kingdom) and 532 nm excitation beams (Sapphire 532 LP, Coherent, Ely, United Kingdom) were combined using a set of dichroic mirrors (Figure S2, Supporting Information). After passing through an acousto-optical tunable filter (AOTF nC-400-650-TN, AA Optoelectronic, Orsay, France), the beam was coupled to an optical fiber (QSMJ-3U3U-488-3.5/125-3AS-3,Oz Optics, Ottawa, Canada) by means of an objective (20 $\times$ /NA 0.4, Olympus, Japan) mounted to an xyz stage (Nanomax 200, Thorlabs, Dachau/Munich, Germany). Inside the microscope, the beam was reflected by a double dichroic mirror (ZT 532/638 rpc, Chroma AHF, Tübingen, Germany) and focused into the microfluidic device using a 4 $\times$  objective (Plan Fluor 4 $\times$ /NA 0.13, Nikon, Zurich, Switzerland). Fluorescence emission originating from individual droplets was collected by the same objective, passed through the Dual-View box and detected with a CMOS camera (ORCA-flash 4.0, Hamamatsu, Solothurn, Switzerland). The Dual-View filter box comprised three mirrors, a dichroic filter (640 DCXR, Chroma AHF, Tübingen, Germany), and two filters (D580/35 and LP655, Chroma AHF, Tübingen, Germany). The two complete images (of different color) were obtained simultaneously using different regions of the CMOS camera array and processed using MicroManager Software (Micro-Manager 1.4, University of California, San Francisco, USA). Synchronization was controlled using an AOTF controller (ESio AOTF Controller, ESImaging, Kent, United Kingdom). The AOTF was triggered by the CMOS camera with a 20 ms TTL pulse to allow synchronization of laser strobing and exposure of the detector.

The sampling frequency of the camera was 50 Hz, and the AOTF driver was set to a pulse length of 1 ms for both laser lines.

**Data Analysis.** ImageJ (1.47v, National Institutes of Health, USA) was used for all image processing. Circular regions of interest (ROIs) with a diameter of 20 pixels (32.5  $\mu\text{m}$ ) and centered at the middle of a droplet were defined in an automated manner using fluorescence originating from the barcoding dye (Figure S3, Supporting Information). Images were flat-field corrected using data recorded under enzyme free conditions, with the ROIs being used to extract the mean intensity of the droplets in both halves of the dual view images. The intensity values of signals from both fluorescent dyes were then archived with droplet position and the corresponding frame number. Knowledge of the droplet velocity (droplet velocities were extracted from high-speed movies) as well as the frame rate was then used to track the droplets through each frame. The substrate concentration inside the droplets was determined by comparing the average emission signal originating from the barcoding dye with a calibration curve. A linear fit was applied to the time dependent signal originating from the reaction product, yielding the initial reaction velocity. The Michaelis constant  $K_m$  was estimated using nonlinear regression analysis.

## RESULTS AND DISCUSSION

A schematic of the complete microfluidic system is shown in Figure 1. The microfluidic device is sectioned into different zones corresponding to specific operations. In zone 1, a concentration gradient is created by varying the relative flow rates of the dilution buffer stream and the barcoded substrate stream. Next, a constant amount of enzyme is added (zone 2) immediately prior to droplet formation at a flow focusing geometry (zone 3). Zone 4 is used to accelerate mixing of droplet contents via chaotic advection. Droplets formed in this way contain a uniform enzyme concentration and variable

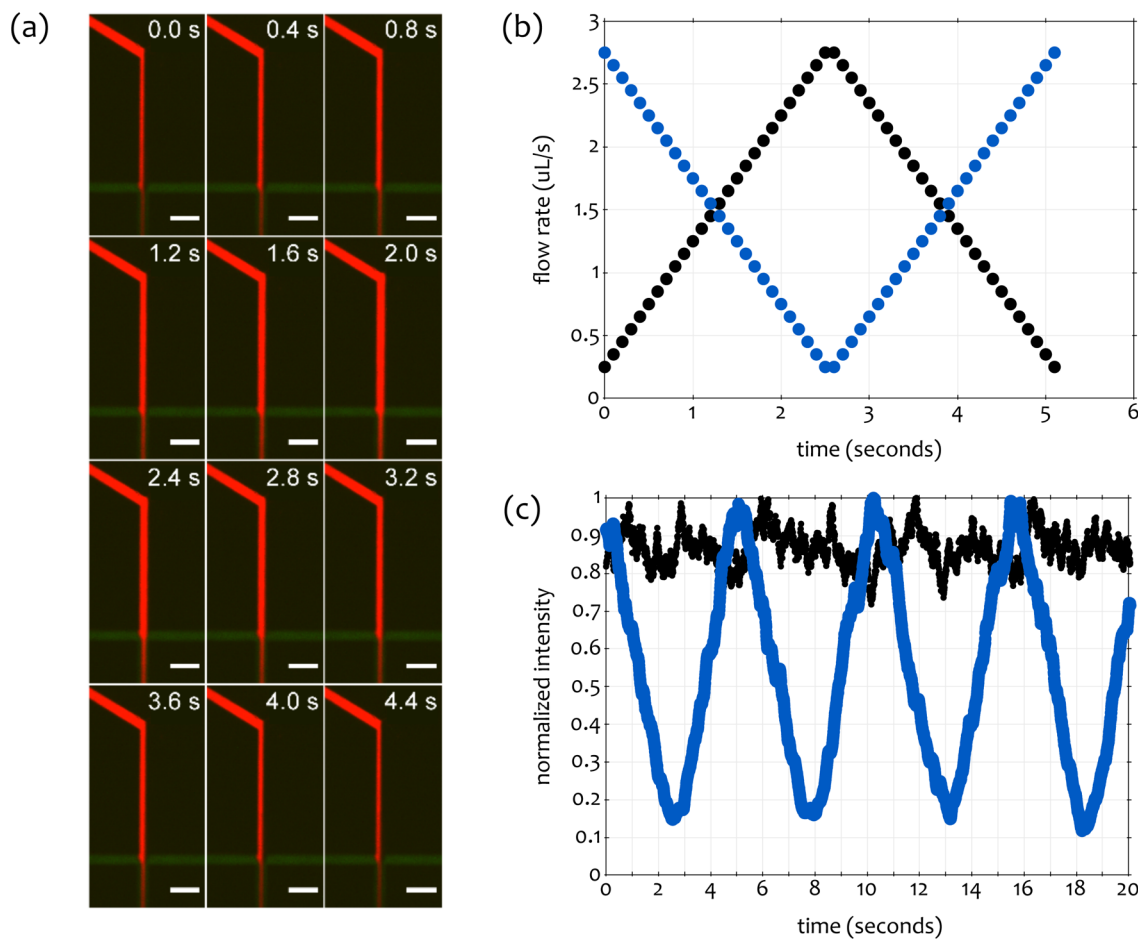


**Figure 2.** Characterization of concentration gradients. (a) An image series showing the dilution of a fluorescent dye (CF 647, red) for an applied triangular flow function with a period of 5 s. The fluorescence signal originating from a resorufin stream introduced at a constant flow rate is visible in green (scale bars are equal to 200  $\mu$ m). (b) Complementary flow profiles applied to the two syringe pumps having a period of 5 s. (c) Extracted fluorescence intensity profiles as a function of time: resorufin, black; CF 647, blue.

substrate concentration. This approach provides for mixing times between 1 and 10 ms.<sup>2</sup> Reactions are subsequently monitored along the serpentine channel where barcoding signals are used to identify individual droplets (zone 5a) with fluorescence originating from the reaction product (zone 5b) being simultaneously detected. While the measured intensity of the barcoding dye can be used to determine the initial substrate concentration for each droplet, the detected fluorescence originating from the converted substrate is used to extract kinetic information. This approach allows for the monitoring of multiple reactions simultaneously at high analytical throughput.

**Generation of Concentration Gradients.** To assay an enzymatic reaction, a variety of experimental conditions, such as the concentration of at least one of the involved reactants, should be screened. The presented method is based on the variation of the relative flow rates of the inlet streams using two complementary and periodic flow functions (or profiles) while keeping the total flow rate constant. Importantly, the method is simple to implement, operationally flexible, and can be used to produce a sequence of droplets that contain varying concentrations of a given reactant. Small fluctuations during the acceleration phase of a pump as well as dispersion (prior to droplet formation) will generate droplets containing concentrations that cannot be directly related to the applied flow profile. This dictates the need to barcode a droplet to provide an index that is directly related to analyte composition. To

overcome possible inaccuracies in creating concentration gradients, droplets were barcoded with Atto 633 ( $\lambda_{\text{ex}} = 633$  nm;  $\lambda_{\text{em}} = 657$  nm). Assuming that both the analyte and the barcoding dye are diluted in the same way, a calibration curve can be used to relate the barcoding signal (Atto 633) to the initial substrate concentration.<sup>18</sup>

To characterize the concentration gradients used in the enzymatic assay, a range of flow profiles were assessed (Figure S4, Supporting Information). For example, Figure 2a shows the creation of a concentration gradient using three inlets that introduce the reagents, the buffer solution, the fluorescent barcoding dye CF 647, and resorufin (Figure S1a, Supporting Information). Several flow profiles were tested to assay the maximum achievable dilution factors, the distribution of droplets with given concentrations of barcoding dye, and the flow stability (fluctuations of added resorufin and variation in droplet velocity) of our microfluidic platform (Figure S5, Supporting Information). Among those tested, profiles based on a triangular function (Figure 2b) demonstrated the best stability in droplet velocity. Accordingly, for the initial experiments, the flow profile depicted in Figure 2b was adopted, allowing for a maximum dilution factor of approximately ten.

**Enzymatic Assay.** A Michaelis–Menten analysis was performed using the enzyme  $\beta$ -galactosidase, an exoglucosidase widely used as a reporter marker in gene expression studies<sup>26</sup>

**Scheme 1.** Hydrolysis of Resorufin  $\beta$ -D-Galactopyranoside (**1**) Is Catalyzed by the  $\beta$ -Galactosidase, Yielding the Fluorescent Product Resorufin (**2**) and D-Galactose (**3**)

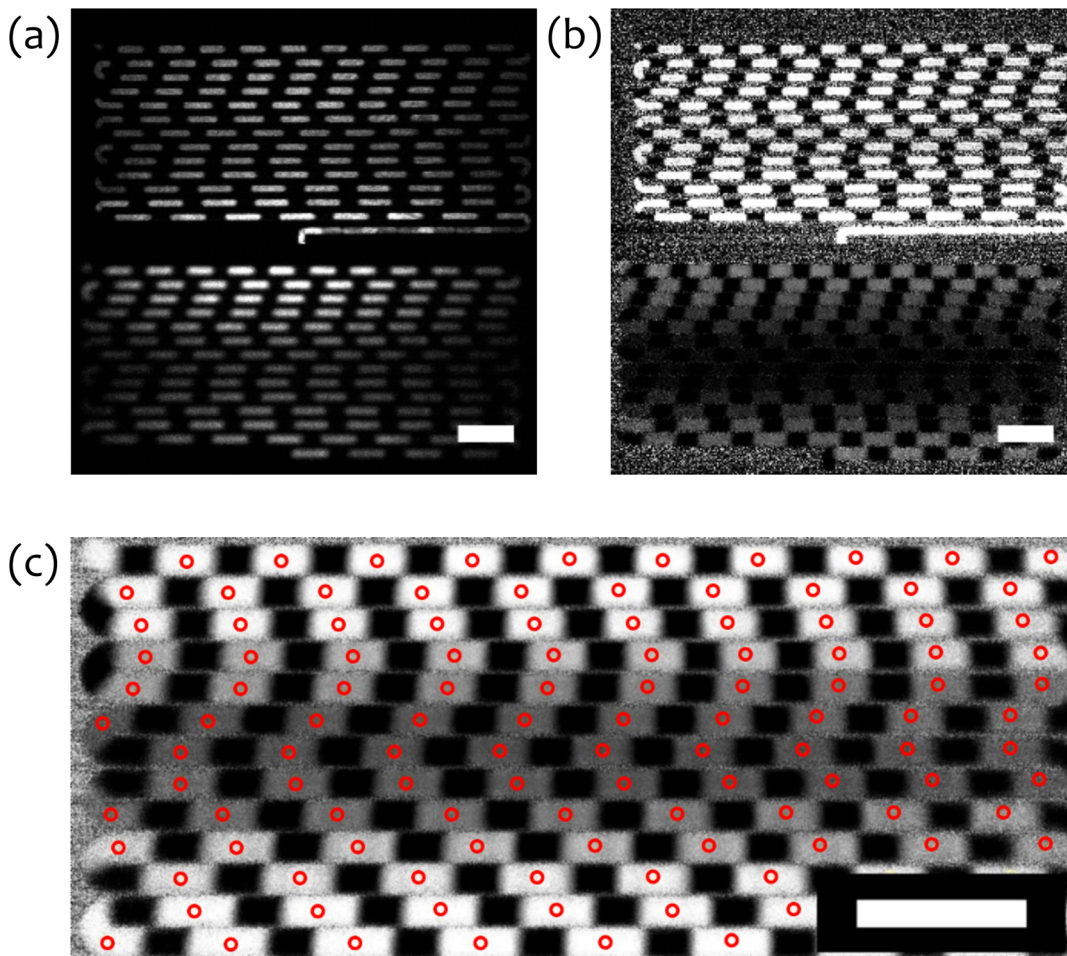
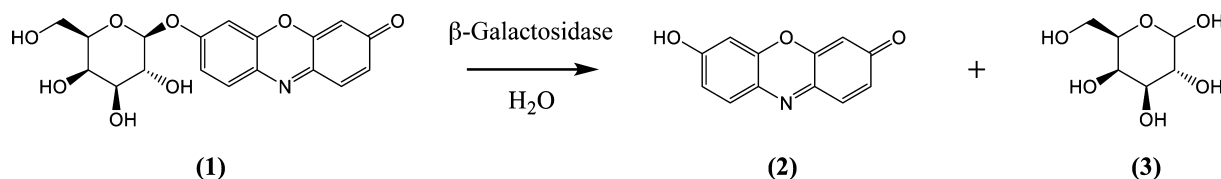


**Figure 3.** Fluorescence imaging of segmented flows. (a) Fluorescence emission originating from resorufin contained within pL volume droplets moving at a velocity of 5 cm/s is shown in the upper half of the image, while emission from the barcoding dye (Atto 633) is shown in the lower half of the image. After application of a flat-field correction, image (b) is obtained. Image (c) shows a contrast enhanced expansion of the lower image in (b), clearly displaying the generated concentration gradient. Red outlines indicate the ROIs where the fluorescence intensities values are extracted. All scale bars are 400  $\mu$ m in length.

and resorufin  $\beta$ -D-galactopyranoside as the fluorogenic substrate. Specifically, hydrolysis of resorufin  $\beta$ -D-galactopyranoside is catalyzed by the  $\beta$ -galactosidase, yielding the products resorufin and D-galactose (Scheme 1). The Michaelis–Menten model assumes that a substrate (*S*) binds to an enzyme (*E*) to generate a complex (*ES*) that is then converted to a product (*P*) with regeneration of the enzyme. The associated rate constants are denoted as *k*<sub>f</sub>, *k*<sub>r</sub>, and *k*<sub>cat</sub>, i.e.,



When  $[S] \gg [E]$ , it is possible to use a quasi-steady-state approximation that yields eq 2, where  $v_0$  and  $v_{\max}$  denote the initial reaction velocity and the maximum reaction velocity,

respectively. The Michaelis constant  $K_m$  is equal to the substrate concentration when the initial reaction velocity is half the maximum value. A nonlinear fit based on this model can be applied to the experimental data to obtain the parameters  $K_m$  and  $v_{\max}$ <sup>27</sup>

$$v_0 = \frac{v_{\max}[S]}{K_m + [S]} \quad (2)$$

The conversion of resorufin  $\beta$ -D-galactopyranoside to resorufin was monitored by tracking each individual droplet as it traverses the field of view. By using a dual view detection scheme, it was possible to simultaneously record the fluorescence of the barcoding dye and resorufin, which allows the direct assignment of the initial substrate concentration for

each droplet (Figure 4a). To take into account the inhomogeneity throughout the field of view, a flat field correction was applied to the raw data (Figure 3a,b). As expected the observed fluorescence intensity of the barcoding dye (which reflects the concentration gradient) closely mimics the applied triangular flow profile (Figure 3c). These results confirm the production of accurate and precise concentration gradients.

As previously noted, owing to the high velocities of the formed droplets (approximately 10 cm/s in the current experiments), droplets must be assayed under high speed imaging conditions. Rapid reactions, therefore, cannot be directly monitored using conventional image-based microscopy, where limits are imposed by the maximum frame rates of commercially available cameras possessing high quantum efficiencies. As a result, the average fluorescence intensity of a series of droplets is typically used to extract the average product concentrations, since individual droplet detection is impossible. In contrast, rapid fluorescence observation of heterogeneous droplets requires the ability to distinguish between individual droplets within the segmented flow. As previously noted, we achieve this using an acousto-optic tunable filter to pulse the excitation light.<sup>28,29</sup> Faster frame rates can only be achieved by shrinking the field of view or by binning pixels. Both approaches reduce the ability to monitor a large number of droplets in parallel. The basic criterion for observing individual droplets is that the distance a droplet travels during a given exposure time must be smaller than the interdroplet spacing. This approach is analogous to stroboscopic photography, in which rapid light flashes allow a rapidly moving object to be observed while the shutter of the camera remains open.<sup>30</sup> Such a reduction in motion blur can be clearly seen in Figure S6, Supporting Information. Since our detection scheme is based on epifluorescence, the progress of reactions in individual droplets can be measured with high temporal resolution without sacrificing the field of view. Since the rolling shutter of the CMOS camera cannot provide clear images of fast moving droplets,<sup>31</sup> we maintained the integration time of the camera at 20 ms but only illuminated for a 1 ms time interval in order to eliminate “streaking” effects. This approach also affords the use of low excitation powers (due to low effective exposure times), thus ensuring minimal fluorophore photobleaching. For dual view detection, the AOTF controlled both violet and red beams simultaneously, which resulted in simultaneous two-color irradiation. Data presented in Figure 4 illustrate signals from individual droplets generated at approximately 150 Hz as they are tracked over time. Information regarding reactions in more than 1400 individual droplets was obtained in a single experiment, by recording images at a frame rate of 50 Hz over a period of 10 s and for substrate concentrations between 60 and 525  $\mu\text{M}$ . Indeed, the fluorescence profiles of individual droplets flowing along the serpentine channel could be directly extracted (Figure 4b). The variation of signal originating from the reaction product (resorufin) increases linearly ( $R^2 > 0.99$ ) with time and reports the progress of the reaction (i.e., conversion of the fluorogenic substrate by the enzyme). It is important to note that the detected fluorescence from the barcoding dye remains constant for each droplet, allowing for a precise assignment of the initial substrate concentration via calibration (Figure S7, Supporting Information), using different but fixed flow rate ratios between buffer and barcoded substrate.

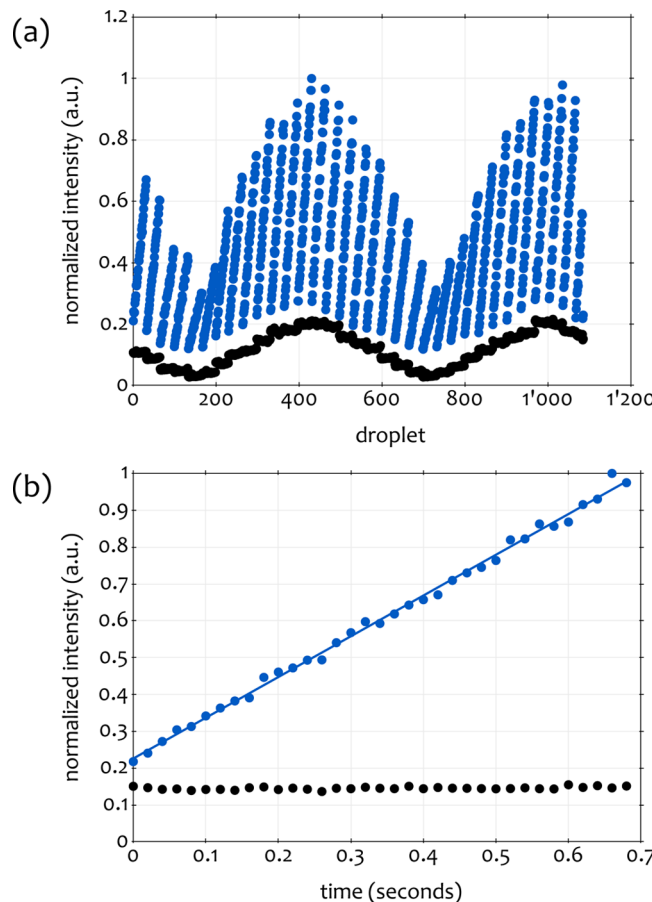


**Figure 4.** Reaction mapping inside individual droplets. The graphical representation (a) shows the measured intensities of the fluorogenic substrate resorufin (blue circles) for every 50th droplet of an experiment passing through the field of view. The measured intensity of the barcoding dye (Atto 633, black circles) indicates the underlying flow profile. In part (b), the situation for a single droplet is shown, including a linear fit ( $R^2 = 0.9965$ ) of the increase in signal (resorufin) over time (frame rate, 50 Hz). The measured intensity originating from the barcoding dye (Atto 633) remains approximately constant and can be related to the initial substrate concentration via a calibration curve.

The initial substrate concentration was plotted against the initial reaction velocity, and data were analyzed by nonlinear regression (Figure 5) to extract  $K_m$  ( $353 \pm 8 \mu\text{M}$ ). This is in excellent agreement with previous literature studies (off chip:  $K_m = 336 \pm 75 \mu\text{M}$ ; on chip:  $K_m = 335 \pm 65 \mu\text{M}$ <sup>32</sup> (100 mM Tris, 2.0 mM KCl, 0.1 mM MgCl<sub>2</sub>, 0.1% BSA, and 0.05% Tween 20 at pH 7.8, RT);  $K_m = 333 \pm 130 \mu\text{M}$ <sup>33</sup> (100 mM Tris, 2.0 mM KCl, 0.1 mM MgCl<sub>2</sub>, 0.1% BSA, and 0.05% Tween 20 at pH 7.8, RT);  $K_m = 442 \pm 99 \mu\text{M}$ <sup>19</sup> (3-(N-morpholino)propansulfonic acid buffer, RT)). Furthermore, it is noted that the current studies provide a denser sampling of the accessible concentration range within a shorter time scale. As shown in the inset of Figure 5, the distribution of the residuals is random indicating that the applied fitting model is appropriate for the aforementioned kinetic assay.

**Inhibition Kinetics.** Inhibitors play a key role in pharmacology since the vast majority of drugs act as enzyme inhibitors that can correct regulatory dysfunctions in disease.<sup>34</sup> Accordingly, powerful tools to study enzyme inhibition kinetics are of high current interest.<sup>35</sup> By using the same experimental

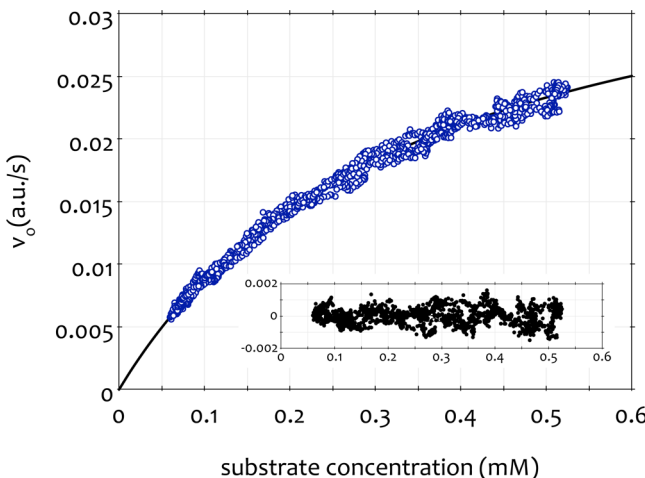


**Figure 5.** Michaelis–Menten kinetics. Initial reaction velocities (calculated from data extracted in a single experiment) as a function of substrate concentration and fitted to eq 2 using nonlinear regression. Inset: Residuals associated with the fit.

approach and a slightly modified microfluidic device (Figure S1b, Supporting Information), it was possible to determine the dissociation constant for the competitive inhibitor isopropyl  $\beta$ -D-1-thiogalactopyranoside<sup>36</sup> (Figure 6a). Data were acquired for 10 different inhibitor concentrations ranging from 4.2 to 75  $\mu$ M. For a competitive inhibitor, the relationship between the observed Michaelis constant ( $K_m^{app}$ ) and the inhibitor concentration ([I]) is linear, i.e.,

$$K_m^{app} = K_m \left( 1 + \frac{[I]}{K_I} \right) \quad (3)$$

and can be used to determine the dissociation constant  $K_I$  (Figure 6b). For isopropyl  $\beta$ -D-1-thiogalactopyranoside,  $K_I$  was determined to be  $63 \pm 7 \mu\text{M}$ , which is in good agreement with the literature value of  $0.08 \text{ mM}$ .<sup>37</sup> By extrapolating to zero inhibitor concentration,  $K_m$  was estimated to be  $342 \pm 66 \mu\text{M}$ , which closely matches experiments conducted without inhibitor.

## CONCLUSIONS

We have presented a novel droplet-based microfluidic methodology for studying enzyme kinetics in a high-throughput manner. By automated manipulation of the flow rates of two fluid streams containing substrate and enzyme, a sequence of droplets defining a substrate concentration gradient can be generated in a direct and rapid fashion. To achieve high-throughput enzymatic screening, this operation is combined with an optical interrogation system that allows the quantification of the enzymatic activity inside individual droplets of varying composition over time. Significantly, our methodology allows the rapid creation of concentration gradients for studying enzyme kinetics without increasing the size or the complexity of the device and simultaneously allowing for ultrahigh-throughput and multiplexed analysis. Specifically, the detection methodology provides for microsecond excitation via stroboscopic illumination, thus allowing the observation of rapid events that are currently inaccessible using conventional wide field fluorescence microscopy. When compared to existing kinetic analysis methods with millisecond time resolution,<sup>25</sup> our optofluidic approach provides two clear

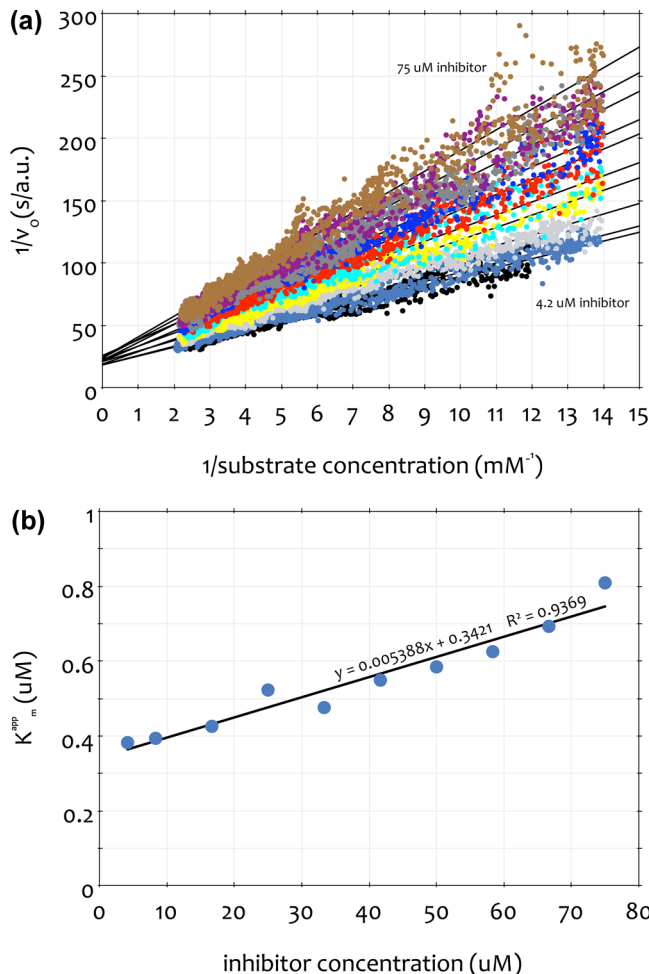


**Figure 6.** Inhibition kinetics: (a) Lineweaver–Burk plot for inhibitor concentrations ranging from 75  $\mu\text{M}$  (top) to 4.2  $\mu\text{M}$  (bottom). (b) Variation of the Michaelis constant as a function of inhibitor concentration.

advantages. First, we are able to sensitively probe a heterogeneous population of discrete droplets due to the ability to track all droplets with high temporal and spatial resolution. Second, we are able to simultaneously measure additional droplet characteristics such as droplet volume, velocity, and shape. The microfluidic platform can be easily adapted to be used for screening of compound libraries<sup>23</sup> as well as for high-throughput cell-based assays.<sup>9</sup> The time-scale range of the platform can be extended by adopting an automated system for scanning multiple regions of an extended observation channel in a serial manner or by integration of a large field of view macro lens.<sup>38</sup>

## ASSOCIATED CONTENT

### S Supporting Information

Additional information as noted in text. This material is available free of charge via the Internet at <http://pubs.acs.org>.

## AUTHOR INFORMATION

### Corresponding Author

\*E-mail: andrew.demello@chem.ethz.ch.

### Notes

The authors declare no competing financial interest.

## ACKNOWLEDGMENTS

The authors would like to acknowledge the Swiss National Foundation, ETH Zürich, and the National Research Foundation of Korea (Global Research Laboratory Programme Grant K20904000004-10A0500-00410) for partial support.

## REFERENCES

- (1) Guo, M. T.; Rotem, A.; Heyman, J. A.; Weitz, D. A. *Lab Chip* **2012**, *12*, 2146–2155.
- (2) Song, H.; Ismagilov, R. F. *J. Am. Chem. Soc.* **2003**, *125*, 14613–14619.
- (3) Cai, L. F.; Zhu, Y.; Du, G. S.; Fang, Q. *Anal. Chem.* **2012**, *84*, 446–452.
- (4) Bui, M.-P. N.; Li, C. A.; Han, K. N.; Choo, J.; Lee, E. K.; Seong, G. H. *Anal. Chem.* **2011**, *83*, 1603–1608.
- (5) Han, Z.; Li, W.; Huang, Y.; Zheng, B. *Anal. Chem.* **2009**, *81*, S540–S545.
- (6) Agresti, J. J.; Antipov, E.; Abate, A. R.; Ahn, K.; Rowat, A. C.; Baret, J.-C.; Marquez, M.; Klibanov, A. M.; Griffiths, A. D.; Weitz, D. A. *Proc. Natl. Acad. Sci. U. S. A.* **2010**, *107*, 4004–4009.
- (7) Granieri, L.; Baret, J.-C.; Griffiths, A. D.; Merten, C. A. *Chem. Biol.* **2010**, *17*, 229–235.
- (8) Koster, S.; Angile, F. E.; Duan, H.; Agresti, J. J.; Wintner, A.; Schmitz, C.; Rowat, A. C.; Merten, C. A.; Pisignano, D.; Griffiths, A. D.; Weitz, D. A. *Lab Chip* **2008**, *8*, 1110–1115.
- (9) Huebner, A.; Srisa-Art, M.; Holt, D.; Abell, C.; Hollfelder, F.; deMello, A. J.; Edel, J. B. *Chem. Commun.* **2007**, 1218–1220.
- (10) Hindson, B. J.; Ness, K. D.; Masquelier, D. A.; Belgrader, P.; Heredia, N. J.; Makarewicz, A. J.; Bright, I. J.; Lucero, M. Y.; Hiddessen, A. L.; Legler, T. C.; Kitano, T. K.; Hodel, M. R.; Petersen, J. F.; Wyatt, P. W.; Steenblock, E. R.; Shah, P. H.; Bousse, L. J.; Troup, C. B.; Mellen, J. C.; Wittmann, D. K.; Erndt, N. G.; Cauley, T. H.; Koehler, R. T.; So, A. P.; Dube, S.; Rose, K. A.; Montesclaros, L.; Wang, S.; Stumbo, D. P.; Hodges, S. P.; Romine, S.; Milanovich, F. P.; White, H. E.; Regan, J. F.; Karlin-Neumann, G. A.; Hindson, C. M.; Saxonov, S.; Colston, B. W. *Anal. Chem.* **2011**, *83*, 8604–8610.
- (11) Krishnadasan, S.; Brown, R. J. C.; deMello, A. J.; deMello, J. C. *Lab Chip* **2007**, *7*, 1434–1441.
- (12) Lignos, I.; Protesescu, L.; Stavrakis, S.; Piveteau, L.; Speirs, M. J.; Loi, M. A.; Kovalenko, M. V.; deMello, A. J. *Chem. Mater.* **2014**, *26*, 2975–2982.
- (13) Macejczyk, R. M.; deMello, A. J. *J. Phys. Chem. C* **2014**, *118*, 20026–20033.
- (14) Cleland, W. W. *Annu. Rev. Biochem.* **1967**, *36*, 77–112.
- (15) Sambrook, J.; Fritsch, E. F.; Maniatis, T. *Molecular Cloning: A Laboratory Manual*; Cold Spring Harbor Laboratory Press: New York, 1989.
- (16) Miller, O. J.; Harrak, A. E.; Mangeat, T.; Baret, J.-C.; Frenz, L.; Debs, B. E.; Mayot, E.; Samuels, M. L.; Rooney, E. K.; Dieu, P.; Galvan, M.; Link, D. R.; Griffiths, A. D. *Proc. Natl. Acad. Sci. U. S. A.* **2012**, *109*, 378–383.
- (17) Damean, N.; Olguin, L. F.; Hollfelder, F.; Abell, C.; Huck, W. T. *Lab Chip* **2009**, *9*, 1707–1713.
- (18) Zheng, B.; Roach, L. S.; Ismagilov, R. F. *J. Am. Chem. Soc.* **2003**, *125*, 11170–11171.
- (19) Sjostrom, S. L.; Joensson, H. N.; Svahn, H. A. *Lab Chip* **2013**, *13*, 1754–1761.
- (20) Jambovane, S.; Kim, D. J.; Duin, E. C.; Kim, S.-K.; Hong, J. W. *Anal. Chem.* **2011**, *83*, 3358–3364.
- (21) Lee, C.-Y.; Chang, C.-L.; Wang, Y.-N.; Fu, L.-M. *Int. J. Mol. Sci.* **2011**, *12*, 3263–3287.
- (22) Srisa-Art, M.; deMello, A. J.; Edel, J. B. *Anal. Chem.* **2007**, *79*, 6682–6689.
- (23) Clausell-Tormos, J.; Griffiths, A. D.; Merten, C. A. *Lab Chip* **2010**, *10*, 1302–1307.
- (24) Srisa-Art, M.; Dyson, E. C.; deMello, A. J.; Edel, J. B. *Anal. Chem.* **2008**, *80*, 7063–7067.
- (25) Chen, C.-H.; Sarkar, A.; Song, Y.-A.; Miller, M. A.; Kim, S. J.; Griffith, L. G.; Lauffenburger, D. A.; Han, J. *J. Am. Chem. Soc.* **2011**, *133*, 10368–10371.
- (26) Hofmann, J.; Sernetz, M. *Anal. Chim. Acta* **1984**, *163*, 67–72.
- (27) Price, R.; Dodds, P. F. *Biochem. Educ.* **1989**, *17*, 138–140.
- (28) Wachman, E. S.; Niu, W.; Farkas, D. L. *Biophys. J.* **1997**, *73*, 1215–1222.
- (29) Bradley, D.; Atcheson, B.; Ihrke, I.; Heidrich, W. Synchronization and Rolling Shutter Compensation for Consumer Video Camera Arrays. In *IEEE International Workshop on Projector-Camera Systems*, 2009; pp 1–8.
- (30) Edgerton, H. E.; Davidhazy, A. *Stroboscopic Photography*. AccessScience. McGraw-Hill Education, 2014 (accessed Apr. 15, 2015).
- (31) Ait-Aider, O.; Andreff, N.; Lavest, J.; Martinet, P. In *Computer Vision – ECCV 2006*; Leonardis, A., Bischof, H., Pinz, A., Eds.; Springer: Berlin Heidelberg, 2006; pp 56–68.
- (32) Jambovane, S.; Duin, E. C.; Kim, S.-K.; Hong, J. W. *Anal. Chem.* **2009**, *81*, 3239–3245.
- (33) Xie, Y.; Ahmed, D.; Lapsley, M. I.; Lin, S.-C. S.; Nawaz, A. A.; Wang, L.; Huang, T. *J. Anal. Chem.* **2012**, *84*, 7495–7501.
- (34) Wong, E.; Okhonin, V.; Berezovski, M. V.; Nozaki, T.; Waldmann, H.; Alexandrov, K.; Krylov, S. N. *J. Am. Chem. Soc.* **2008**, *130*, 11862–11863.
- (35) von Ahsen, O.; Bömer, U. *ChemBioChem* **2005**, *6*, 481–490.
- (36) Herzenberg, L. A. *Biochim. Biophys. Acta* **1959**, *31*, 525–538.
- (37) Juers, D. H.; Rob, B.; Dugdale, M. L.; Rahimzadeh, N.; Giang, C.; Lee, M.; Matthews, B. W.; Huber, R. E. *Protein Sci.* **2009**, *18*, 1281–1292.
- (38) Hatch, A. C.; Fisher, J. S.; Tovar, A. R.; Hsieh, A. T.; Lin, R.; Pentoney, S. L.; Yang, D. L.; Lee, A. P. *Lab Chip* **2011**, *11*, 3838–3845.